NASA TECHNICAL NOTE

NASA TN D-4874

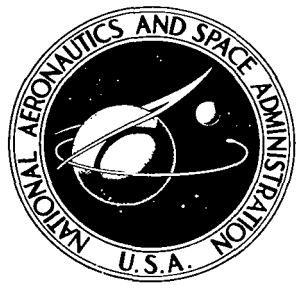

NASA TN D-4874

SUMMARY OF ELECTRICAL COMPONENT DEVELOPMENT FOR A 400-HERTZ BRAYTON ENERGY CONVERSION SYSTEM

by Charles S. Corcoran and LeRoy J. Yeager

Lewis Research Center
Cleveland, Ohio

NATIONAL AERONAUTICS AND SPACE ADMINISTRATION • WASHINGTON, D. C. • NOVEMBER 1968

SUMMARY OF ELECTRICAL COMPONENT DEVELOPMENT FOR A 400-HERTZ BRAYTON ENERGY CONVERSION SYSTEM

By Charles S. Corcoran and LeRoy J. Yeager

Lewis Research Center
Cleveland, Ohio

NATIONAL AERONAUTICS AND SPACE ADMINISTRATION

For sale by the Clearinghouse for Federal Scientific and Technical Information
Springfield, Virginia 22151 – CFSTI price $3.00

ABSTRACT

The major electrical components of a 400-hertz Brayton-cycle system are the alternator, the voltage regulator - exciter, and the parasitic-loading speed controller. Unique design features of the components are described. The experimental evaluation of the components and subsystem indicates that the alternator has an efficiency of 91.5 percent at design and that the steady-state and transient performance is suitable for a space power system. In addition, bearing reactions caused by magnetic unbalance resulting from an unsymmetrical gap were determined experimentally. The data show that the reactions consist primarily of a constant and a pole-frequency component.

SUMMARY OF ELECTRICAL COMPONENT DEVELOPMENT FOR A 400-HERTZ BRAYTON ENERGY CONVERSION SYSTEM

by Charles S. Corcoran and LeRoy J. Yeager*

Lewis Research Center

SUMMARY

The development of a 12-kilowatt inductor alternator, a voltage regulator - exciter, and a parasitic-loading speed controller designed for high reliability and efficiency is described. The development consisted of design, fabrication, and experimental verification, including a test program to determine bearing reactions caused by magnetic unbalance. Unique alternator design features include laminated pole tips, amortisseur windings, and polyimide film insulation. The speed controller utilizes multiple parasitic loads to reduce harmonic distortion and silicon controlled rectifiers (SCR) to minimize turnoff losses.

The alternator is 91.5 percent efficient at design conditions. The magnetic unbalance tests show that there is a speed, or frequency, effect which reduces the forces. For eccentricities less than 15 percent of the airgap (0.002 in. (0.005 cm)), the bearing reaction is less than 7 pounds (30 N). The resultant forces are primarily a constant radial force and a time-varying component at rotor-pole frequency.

INTRODUCTION

The purpose of this report is to summarize the design and the developmental testing of the alternator, the voltage regulator - exciter, and the speed controller required for a two-shaft, Brayton-cycle power system (refs. 1 to 3). Prior to this work, the electrical components for the 35-kilowatt SNAP-8 system (refs. 4 and 5) were developed. This experience contributed significantly to the development of the Brayton-cycle electrical components. Several unique approaches were incorporated in the Brayton-cycle electrical system to enhance its reliability and efficiency. And for the first time gas bearings were

*Mr. Yeager is with the General Electric Company, Erie, Pennsylvania.

used in a turboalternator designed for use in space. The gas bearings required minimization of the unbalanced flux in the gap to minimize the resulting forces. The data reported herein were obtained from an electromagnetic-equivalent alternator operating on oil-lubricated rolling-element bearings. This report summarizes the design and performance of the electrical system (refs. 6 to 11) and includes the motor-start characteristics of the alternator.

Throughout the design phase of the program, reliability was assigned the highest priority, followed by the effort to maximize efficiency. The emphasis on high reliability was the result of the anticipated, unattended operating life of five years. Efficiency was emphasized to deliver the maximum amount of power and because the weight of the electrical components is small in comparison with the remainder of the system. Performance and weight were considered to have approximately equal importance and to be of less significance than reliability and efficiency.

The experimental phase of this program included the determination of steady-state performance, transient performance, and efficiency at both design and off-design conditions. In general, the approach consisted of the experimental evaluation of each component and the integration of components to form a subsystem.

ALTERNATOR

Design

The Brayton-cycle alternator (refs. 6 and 8) is a four-pole homopolar inductor machine operating at 12 000 rpm to produce 400-hertz power at 120/208 volts. It is rated 12 kilowatts at 0.8 power factor with 93° C coolant. The machine is sealed to prevent loss of argon which is the working gas in the system. Figure 1 is a sectional view of the test alternator. The field coil located between the two stator stacks produces a unidirectional flux. The action of the poles is to rotate this flux in reference to the armature coils. The total effect is a pulsating, unidirectional flux in the armature coils located in the two stator stacks and constant unidirectional flux in the frame and rotor. A Fourier analysis of the pulsating flux shows a constant component, a fundamental, and all odd harmonics. Since no voltage is induced in the armature winding by the constant flux, the induced voltage consists of the fundamental and the odd harmonics. As with conventional machines, the voltage harmonics can be minimized by the winding arrangement. Since the fundamental of the Fourier analysis is periodic, this analysis indicates that at each end of the machine there are virtual poles of opposite polarities between the real poles. The final result is that the voltage induced at each end of the machine is periodic and in time phase with the rotor. The alternator has laminated pole tips and amortisseur windings, both of which are unique to machines of this type. The laminated pole tips,

which were electron-beam welded to the rotor, were incorporated in order to minimize the pole-face loss due to eddy currents. The amortisseur windings serve to equalize the voltage during unbalanced loading conditions.

Another unique feature for machines of this type was the use of polyimide film insulation entirely around each coil side in the slot to improve the dielectric characteristics. In addition, the ground and conductor insulation was entirely polyimide, utilizing film for the ground and enamel for the conductor. A silicone glass separator was used between coil sides, primarily to ease the winding operation.

Table I summarizes the final design of the alternator. In general, the design is conservative in that it is based on materials and techniques that are well established. Unique design features and materials were selected only when a significant increase in reliability, efficiency, or performance would be realized.

Two features of the design serve to reduce the unbalance of flux. Because the gap is about twice the airgap in conventional aircraft alternators, any asymmetry yields about one-half the unbalanced flux. Second, the armature winding consists of two separate windings connected in parallel and displaced by 360 electrical degrees, or 180 mechanical degrees. The effect of these parallel or double-circuit windings is to provide a path for the flow of compensating currents, which serves to reduce the unbalance.

Performance

For measurement of electrical performance, a test alternator was fabricated (referred to as alternator research package (ARP) in refs. 6 to 8). Although the test alternator duplicates the electrical and magnetic characteristics of the final alternator, the gas bearings were replaced by ball bearings and, accordingly, the end bells were changed. Figure 2 shows the rotor of the test alternator. The pole faces, amortisseur windings, and windage baffles are evident. Figure 3 shows the rotor for a turboalternator with the large shaft required by the gas bearings. Figure 4 shows the rotor and laminated pole faces prior to electron-beam welding and final machining. It is evident that substantial axial length and diameter are required for the gas bearings. Each assembled rotor was subjected to a spin test at 20 000 rpm, or 167 percent of rated speed, for 5 minutes at 260° C. After the spin test, each rotor was checked for dimensional and balance changes. In figure 5 the alternator stator, as well as the electrical terminals and a coolant passage header, is shown.

Figures 6(a), (b), and (c) are the characteristic and saturation curves. The degree of saturation in the alternator can be noted by observing in figure 6(a) that 2.7 field amperes are required to produce the rated 120 volts at no load. In figure 6(b) the rated, or 1 per unit load, at 0.8 lagging power factor requires 5.7 field amperes, an increase of 3 amperes. To reach double, or 2 per unit, load the field current must be increased by 4.1 amperes to reach the necessary 9.8 field amperes. However, these data indicate

that double load is within the magnetic capability of the alternator. Figure 6(c) shows the saturation curves for 1-power-factor loads. A comparison of figures 6(b) and (c) shows that the field-current requirements are significantly reduced when the power factor is increased. During normal operation, transients of approximately 200 percent net load may be applied to the alternator by the speed-control system.

The losses computed from design data and the measured losses are compared in table II. The net efficiencies compare favorably, but there are significant differences in the loss distribution. Field copper loss is lower than calculated because both field current and temperature are lower than predicted. The higher core loss probably reflects the effect of stator-bore grinding, which tends to smear and short the laminations. This increases eddy-current loss. This grinding operation was necessary in order to obtain a uniform gap between the rotor and the stator and thus minimize the unbalanced magnetic force. A similar operation on the rotor periphery probably increased the pole-face loss and resulted in higher core and stray-load losses. However, secondary effects, such as flux harmonics, might also be contributing factors. Windage losses were estimated from experimental data from similar rotor configurations both with and without windage baffles. The Brayton-cycle rotor configuration was sufficiently different and the baffle test data were sufficiently conservative that windage losses were lower than expected.

In figure 7, efficiency is plotted as a function of alternator output for a coolant temperature of 93.4° C. Since core loss is essentially independent of load, it becomes the predominant loss at low power while the stator- and field-copper losses become predominant at high power. These two effects act to keep the efficiency quite flat over a large power range. When the coolant temperature was reduced from 93.4° to 26.7° C, the level being considered in more recent system configurations, the generator efficiency increased by about 0.5 percent. This increase in efficiency is due primarily to the reduced resistance of the armature and field copper.

When heat runs were made on the alternator using MIL-7808 oil as the coolant, thermocouples located at the end turns and on the interconnecting buses showed the highest readings. The data presented in figure 8 indicate that the thermal design is conservative because of the use of large copper and iron sections to obtain high efficiency at rated load.

Since the alternator appeared to be conservative both electromagnetically and thermally, consideration was given to the means by which this margin could be utilized to improve the efficiency, reduce the weight, or simplify the fabrication. The following are some specific areas of improvement and the resulting tradeoffs that were considered:

(1) The alternator as designed and fabricated could be operated at a higher power level. The results would be a slightly reduced efficiency and a decrease in overload capability.

(2) The alternator could be redesigned to a lower power level. The results would be similar to operating the original machine at a higher power level in that both the

efficiency and overload capability would be decreased. However, the machine weight would also decrease.

(3) Weight could be saved by reducing the outside diameter of the laminations. This would have no appreciable effect on performance, but the fabrication would be considerably more complex.

(4) If the laminated pole tips were abandoned, the fabrication would be greatly simplified. In this case, however, the pole-face loss would increase to about 150 watts and efficiency would drop about 1 percent. As a result the rotor would become significantly hotter.

(5) Consideration was also given to use of different materials. Again the tradeoff was a reduction in weight against reductions in efficiency and overload capability. It was believed that improvement in any area would have a degrading effect in some other area.

Insulation life is dependent on temperature and is the only significant wear-out mechanism in alternators of this type. Because of the high efficiency and resulting low temperatures, the goal of high reliability was apparently achieved. This success was due to the relatively large conductors and generous iron sections which resulted in low current and flux densities.

Motor Starting

No data on the motoring characteristics of inductor machines appear in the literature. However, the construction of the inductor machine is such that current is induced in the amortisseur winding from the armature current and its associated flux. The current in the amortisseur windings also produces flux. The reaction of the two flux waves produces a torque so that induction-motor starting is accomplished. To provide experimental data, the alternator was started as an induction motor with electric power supplied by an existing 40-kilovolt-ampere, 400-hertz, three-phase, 120/280-volt turbine alternator. During the run the voltage varied between 104 and 112 volts as a result of the regulation of the turbine alternator and the voltage drop in the cables. The acceleration time from 0 to 12 000 rpm was 3.3 seconds. Current, voltage, and speed were measured directly against time. Torque was computed from angular acceleration and inertia. The reduced data are shown in figure 9, where the dashed curve shows the data corrected to 110 volts. The performance does not approach that of a comparable induction motor. However, the torque at zero speed is approximately 50 percent of the design full-load torque as a generator. The data indicate that motoring of the alternator is a feasible method for starting a single-shaft, Brayton-cycle power system, in which the turbine, alternator, and compressor are on a common shaft. By motoring the alternator, all the rotating components would be accelerated simultaneously until a self-sustaining speed was attained.

BEARING FORCES DUE TO MAGNETIC UNBALANCE

Gas bearings, operating with very small clearances, inherently have a low tolerance to overloads. Because the bearings also have very low damping, forces tending to excite rotor vibration are important. Therefore, the magnitude and frequency of the forces must be known for design of a reliable bearing system. In the specific case of an alternator operating on gas bearings, unbalanced magnetic fluxes produce forces on the pole faces which must be restrained in the bearing system. Under ideal conditions, all magnetically produced forces in electrical machines cancel out and only the torsional component remains. However, such factors as manufacturing tolerances and misalinement of the rotor in the stator bore can and do cause unbalanced magnetic flux and a resultant unbalanced radial force. However, such compensating factors as currents in the armature winding, the pole faces, and the amortisseur winding tend to reduce the seriousness of the problem. These currents, in accordance with Lenz's law, produce fields which act to oppose the unbalanced flux. Furthermore, saturation in the iron is another effect which reduces the flux unbalance. To date, the problem has eluded a rigorous, quantitative analysis. However, a solution to a specific problem could be obtained experimentally.

It was determined that the displacement of the rotor axis from the centerline of the stator bore is representative of all conditions causing magnetic unbalance. In addition, the displacement, or eccentricity, of the rotor in the stator bore could be readily controlled in the test rig. In the resulting test program bearing reactions were measured as functions of rotor displacement with load and fault conditions as parameters (ref. 11).

The experimental apparatus consisted of a test alternator with antifriction bearings and special end supports, designed so that the bearing reactions could be measured. Four sets of end supports were fabricated. By changing end supports the eccentricity could be set at approximately 0, 0.002, 0.004, and 0.006 inch (0, 0.005, 0.010, and 0.015 cm) with respect to the nominal gap of 0.040 inch (0.1 cm). The struts, which are the most critical parts of the assembly, are shown in figure 10. Each end support consists of an outer ring, four struts, and the bearing housing. The end-support system was fabricated entirely from nonmagnetic 304 stainless steel. The cross-sectional area of the struts was minimized in order to give a measurable strain while the length in the axial direction provided strength to withstand the bearing axial preload. With strain gages mounted on either side of the strut, any bending caused by torsional forces was cancelled in the instrumentation system. In addition, the instrumentation system was biased to cancel out the response caused by rotor weight.

The transmissibility (i.e., the ratio of the force measured on the rotor to the force applied to the stator) as a function of frequency was determined experimentally on a shaker table. These data are shown in figure 11 and are typical of a spring mass system with damping. Unfortunately, the resonance occurred at 400 hertz, which is the same as

the electrical or pole frequency. Furthermore, this is the precise frequency of the anticipated bearing reactions. An alternate approach to this problem was therefore investigated.

A test was conducted at reduced speed at an eccentricity of 0.004 inch (0.010 cm) with rated field current (2.7 A) to produce rated flux. The resultant maximum instantaneous force as a function of speed is shown in figure 12. These results clearly indicate that there is a significant speed effect at very low speeds and that force is essentially constant at speeds between 1000 and 3000 rpm. The form of figure 12 can be qualitatively analyzed as follows:

(1) At standstill, there are no time-varying fluxes or currents. The unbalanced flux produces a force as in the classical electromagnet. This force is the result of the unbalanced flux only since the bearing reactions caused by rotor weight have been cancelled out in the instrumentation system.

(2) As the machine begins to rotate, voltages resulting from the unbalanced flux are generated in the armature and amortisseur windings. These voltages and the resulting currents are directly proportional to the unbalanced flux and the speed. (At very low speeds, the reactance is negligible.) The currents, in turn, produce fluxes which counteract the unbalanced flux. This accounts for the linear decay in force.

(3) As the machine speed increases, the current is determined by the impedance Z where $Z = \sqrt{R^2 + X^2}$ and where R is resistance and the reactance X is proportional to the inductance and the frequency. As the frequency (or speed) increases, the reactance becomes more significant and the rounded portion of the curve is produced.

(4) As the machine speed and frequency increase further, the impedance is determined by the reactance. Since both the voltage and the impedance are proportional to speed, the current and the resulting counteracting flux are constant.

Based on the test results and the qualitative analysis, the experimental program was conducted at 3000 rpm, which placed the bearing-mass system in a regime with transmissibility equal to 1. As a result of the speed reduction, the output voltage was reduced to 25 percent of the design value. The machine was then loaded to provide the flux and armature current at the following test conditions:

(1) The equivalent of a 15-kilovolt-ampere, 0.8-power-factor, balanced three-phase load

(2) The equivalent of a 11.25-kilovolt-ampere, 0.8-power-factor, balanced three-phase load

(3) The equivalent of a 3.33-kilovolt-ampere, 1-power-factor, single-phase load

(4) Three-phase fault with the machine preloaded with the equivalent of a 15-kilovolt-ampere balanced load

(5) Single-phase fault to ground with the machine preloaded with the equivalent of a 15-kilovolt-ampere balanced load

Two sets of experimental data were taken with load and eccentricity as variables. The first consisted of Lissajous figures at the drive and opposite ends of the alternator. For this set of data, all frequencies above the third harmonic (300 Hz) were filtered out. The second set of recorded data consisted of the constant force, the fundamental, and the second and the third harmonics of the strain-gage output. In the data reduction, the time-varying responses were superimposed on the constant-force component. Figures 13(a) and (b) are typical of the reduced data and show the results for the balanced 15-kilovolt-ampere load and for the single-phase faults.

Maximum bearing reactions determined from the Lissajous figures are summarized in figure 14 for various eccentricities and loads. The equivalent loads refer to the fact that the armature current and flux are equal to the rated values but that the voltage is 25 percent of rated because of the reduced speed. These data indicate that for eccentricities less than 0.002 inch (0.005 cm), or 5 percent of the gap, the maximum force is less than 7 pounds (30 N). The tolerances on the stator bore and rotor outside diameter were strictly controlled to limit the gap eccentricity to 0.001 inch (0.003 cm). Since the poles at each end of the machine are identical, it was expected that the bearing reactions would be similar. However, the linearity differs between the drive and opposite ends of the machine. This difference could be caused by second-order effects such as axial displacement of the rotor in the stator bore and flux caused by end leakage. In addition, it is obvious that faults, either three-phase or single-phase, cause greater bearing reactions than single-phase or balanced three-phase loads.

Further analysis of the bearing-response data leads to the following observations:

(1) As expected, the fundamental and the harmonics in the vertical and horizontal directions were equal.

(2) Except in the case of the single-phase fault, the second and third harmonics were small or nonexistent.

(3) For single-phase faults, the magnitude of the second and third harmonics approached the magnitude of the fundamental.

(4) The time-varying response of the system was approximately equal for three-phase faults and the equivalent of 15 kilovolt-amperes. However, the constant-force component increased significantly when the fault was applied.

(5) In all cases the force was toward the bottom of the machine, which is toward the short gap. However, there was also a horizontal component.

With the eccentricities anticipated in the alternator and with the capability of the bearing system, these measured unbalanced forces are entirely acceptable. Further, since all frequencies are greater than the rotational frequency, the excitation for subsynchronous whirl is not present.

VOLTAGE REGULATOR - EXCITER AND TRANSIENT VOLTAGE PERFORMANCE

The voltage regulator - exciter (VRE)(refs. 7 and 8) is shown in diagrammatic form in figure 15. The VRE consists of the sensing circuit, two amplifier stages, the saturating-current potential transformer (SCPT), and a feedback or stabilizing network. The sensing circuit provides a dc voltage proportional to the average of the three input phase voltages. In the case of severe over-voltages on one phase, usually caused by unbalanced faults, a "highest-phase-takeover" circuit assumes control. The output of the sensing circuit is compared with a zener-diode reference voltage. The difference voltage is then amplified by a transistor and magnetic amplifier. The dc output current of the magnetic amplifier provides control for the SCPT.

The SCPT is a three-phase transformer with two input windings, one fed by the line current and one fed by the line voltage that has been shifted approximately 90^{o} with linear reactors. The other windings are an output winding and a control winding. The winding fed by the line current provides a magnetomotive force that is proportional to the load current and will provide alternator-field current during short circuits. At any constant-volt-ampere load, an alternator requires more field current as the lagging power factor decreases. The reactors then shift the phase of the voltage such that the total flux in the SCPT and therefore the output are greatest at low power factor. The output voltage of the SCPT can be decreased to approximately zero by increasing the control current. The output of the SCPT is rectified and applied to the alternator field.

Figure 16 shows the breadboard VRE designed for rack mounting. All data reported herein were obtained with this apparatus.

To determine the transient performance of the regulator, loads were applied to and removed from the alternator. Figures 17 and 18 shows the effect of a step change in load for both 0.8 and 1 power factors. The magnitude of the voltage transient (fig. 17) is inversely related to the power factor and directly related to the magnitude of the load change. For instance, with a 1 per unit total change in load at 0.8 power factor, the voltage rise will not exceed the rated value by more than 28 percent or dip below rated value by more than 23 percent.

Voltage recovery time (fig. 18), as expected, varies inversely with the power factor and directly with the magnitude of the load change. The voltage recovers from a 1 per unit, 0.8-power-factor, step change in load within 170 milliseconds.

The losses of the voltage regulator - exciter for various loads and power factors (fig. 19) are between 45 and 85 watts in the range of greatest interest, compared with the design prediction of 94 watts. At the design point, the combined efficiency of the alternator and VRE is 0.07 percent lower than for the alternator alone, and the effect of the VRE increases as the load decreases. To determine the net input, it was necessary to measure the difference between the input to the VRE and the output to the system load. Both these values are large, and the difference is equal to the sum of the losses and the

output to the alternator field. A unique method (ref. 2) was devised to accomplish this measurement. Mathematically this difference is

$$\text{Alternator output power - Load power = Field power + VRE losses} = 3\left[(V_1 - V_2)(I_1)\cos\theta_A + (I_1 - I_2)V_2\cos\theta_B\right] \quad (1)$$

where

V_1 input voltage

V_2 output voltage

I_1 input current

I_2 output current

θ_A phase angle between I_1 and $(V_1 - V_2)$

θ_B phase angle between V_2 and $(I_1 - I_2)$

Both these values are of about the same magnitude and are readily measurable.

The alternator and VRE provide good transient performance to limit voltage excursions and minimize voltage recovery time. The VRE has low loss which maximizes the efficiency of the alternator and VRE as a subsystem.

SPEED CONTROL

A parasitic-loading type of speed control (refs. 9 and 10) was selected for the Brayton-cycle system to eliminate the need for moving control elements in the gas system and to prevent transient and steady-state pressure drops in the thermodynamic system. A parasitic-loading speed controller consists of a resistor connected in parallel with the useful load. The power delivered to this parallel, or parasitic, resistor is controlled in order to balance the alternator input and output powers so that the rotational speed is essentially constant. However, this type of speed control, operating in the phase-controlled mode, imposes a penalty on the alternator because of the generation of harmonic currents. Gilbert (ref. 12) has investigated this problem analytically. He concludes that the use of multiple parasitic loads, in place of a single equivalent parasitic load, significantly reduces the harmonic distortion of the output voltage waveform and the volt-ampere demand on the alternator. The effects of the number of parasitic loads on the total harmonic content and relative apparent power, or volt-amperes, are shown in figures 20 and 21. The useful power in both cases is at a power factor of 0.80. Figure 20 shows that the maximum total harmonic distortion can be reduced from 0.32 to 0.18 by dividing the parasitic load into two sections. The total harmonic distortion is

further reduced to 0.12 when the parasitic load consists of three sections. In the limit, that is with an infinite number of parasitic loads, there is no distortion. Figure 21 shows that with one parasitic load the maximum relative apparent power demand on the alternator is 1.075; that is, 7.5 percent greater volt-ampere capacity is required with a single parasitic load than with no parasitic load. When two parasitic loads are utilized, the relative apparent power is reduced to 1.03; that is, only 3 percent more capacity is required with two parasitic loads than with no parasitic load. The increases in apparent power are caused by increased harmonic currents which effectively decrease the power factor. An increase in apparent power results in a larger alternator which must be sized to accommodate the increased current and flux. For the Brayton-cycle application, three parasitic loads were selected. Two parasitic loads were utilized for full alternator capacity, which is equivalent to the two parasitic loads of figure 20. A third parasitic load was added to provide redundancy and to improve the transient response. The minimum value of parasitic load that will control the turboalternator speed over the load range is 100 percent of the turboalternator power. With three speed-control units, one of which is considered to be redundant, the total parasitic load should be capable of absorbing at least 150 percent of the system power. Studies of speed decrement characteristics (ref. 10) indicate that 150 to 200 percent load optimizes the system. Since the system is rated at 10 kilowatts, as opposed to the alternator 12 kilowatts, a parasitic load of 18 kilowatts was selected. In addition to the reduction in harmonics, the use of three parasitic loads has the following advantages:

(1) By connecting one sensing circuit to each phase of the alternator, at least a portion of the parasitic load is functional during single-phase faults and open circuits.

(2) The total parasitic load is sized to function when one of the three parallel loads is inoperative.

The speed controller, as shown in figure 22, consists of three complete and separate sections. Each responds to a slightly different generator frequency band. By this technique, only one section is contributing to the generation of harmonics; the other two are either full on or full off. This technique was somewhat relaxed in order to provide for smooth transition from one to the other, resulting in a slight amount of overlap between sections. As shown in the block diagram, each section consists of a discriminator, a magnetic preamplifier, a magnetic amplifier triggering stage, and the SCR power stage. Silicon controlled rectifiers were used in this application to minimize turn-off losses and response time. The sensing circuit consists of two stagger-tuned circuits, which provide high gain over a narrow frequency range with the characteristic of a sharply tuned resonant circuit. The control functions over one-half of the bandwidth since the response tends to reverse as the frequency passes through resonance. In this application, an overspeed subcircuit was incorporated to compensate for the high-frequency reversal.

Since the Brayton-cycle turboalternator was not available, the breadboard speed control was operated on an existing 400-hertz 6000-rpm turboalternator. The inertial

time constants of the two turboalternators were sufficiently close that they could be equalized by adjusting the alternator operating power of the existing 6000-rpm machine to 13.8 kilowatts, somewhat above the Brayton-cycle power rating of 10 kilowatts.

Figure 23(a) summarizes the steady-state performance of the speed controller as obtained from turboalternator tests. The solid curve indicates that the control will maintain load from 400 hertz to any possible overspeed condition. The dashed curve shows the deviation of the response when the overspeed circuit is disconnected. These data indicate that the speed controller could be operated without the overspeed control only if an overspeed trip were incorporated into the protection in order to initiate a shutdown whenever the frequency exceeded 450 hertz.

Figure 23(b) is an expanded response curve in the frequency range of 400 to 407 hertz. In addition the figure shows the response when the second parasitic load is inoperative. Both curves shown in figure 23(b) have continuous, positive gain as required for stable operation. The effect of overlapping the sections is particularly evident when the second parasitic load is off. The loss of the first load bank shifts the frequency set point and reduces the maximum parasitic load, whereas the loss of the third load bank merely reduces the maximum parasitic load.

Figures 24(a) and (b) describe the transient response of the system to step changes of 100 percent load. The data show that the system is stable and underdamped. Of particular significance is the performance when 100 percent load is added to the system. The parasitic load decreases as a function of the turboalternator speed and continues to decay below 400 hertz. The causes of this behavior are the decrease in turbine power with speed and the time lag of the speed controller, which momentarily leaves an increment of load on at 400 hertz. One solution to the problem is to operate with a surplus power margin, low enough to limit the magnitude of the load that can be switched on to a value that will control the speed undershoot to a small amount. When the turboalternator output power was adjusted to 14.5 kilowatts and the useful load of 13.8 kilowatts (95 percent of the output power) was switched on, the frequency decreased to 400 hertz and then recovered to a stable operating point, as shown in figure 24(b).

Under these test conditions, the speed controller was stable when the system was subjected to load step changes of 13.8 kilowatts. In all cases the system reached a stable operating point within 0.6 second. In addition, the system performed in a satisfactory manner with any one of the three speed-control sections inoperative.

SUMMARY OF RESULTS

The electric components of the 400-hertz Brayton-cycle system demonstrated high efficiency and, when connected in subsystems, stable transient performance. In particular, the alternator is approximately 91.5 percent efficient under design conditions and

slightly more efficient when operated at a lower system temperature. Unique design features in the alternator include laminated pole tips, amortisseur windings, and polyimide film insulation.

In regard to magnetic unbalance forces, the following conclusions were reached:

1. There is a speed (frequency) effect which reduces the forces significantly as the speed is increased from standstill.

2. For eccentricities less than 0.002 inch (0.005 cm, or 5 percent of the airgap), the bearing reaction is less than 7 pounds (30 N).

3. For normal load and balanced faults, the forces consist of a constant force and a pole-frequency component.

4. For single-phase faults, the magnitude of the second and third harmonics approaches the magnitude of the fundamental.

The voltage regulator - exciter acts to limit the voltage recovery time to 170 milliseconds for a 1 per unit, 0.8 power-factor step change in load. At the design point, the combined efficiency of the alternator and VRE is 0.07 percent lower than for the alternator alone. The speed control is unique in the use of silicon controlled rectifiers and multiple parasitic loads. The use of silicon controlled rectifiers leads to low turn-off losses and fast response. Multiple parasitic loads make possible a reduction in harmonics and a reduction in the volt-ampere demand on the alternator.

Lewis Research Center,
National Aeronautics and Space Administration,
Cleveland, Ohio, June 20, 1968,
120-27-03-42-22.

REFERENCES

1. Glassman, Arthur J.; and Stewart, Warner L.: A Look at the Thermodynamic Characteristics of Brayton Cycles for Space Power. Paper No. 63-218, AIAA, June 1963.

2. Stewart, Warner L.; Glassman, Arthur J.; and Krebs, Richard P.: The Brayton Cycle for Space Power. Paper No. 741A, SAE, Sept. 1963.

3. Hurrell, Herbert G.; and Thomas, Ronald L.: Control and Startup Considerations for Two-Spool Solar-Brayton Power System. NASA TM X-1270, 1966.

4. Repas, David S.; and Valgora, Martin E.: Voltage Distortion Effects of SNAP-8 Alternator Speed Controller and Alternator Performance Results. NASA TN D-4037, 1967.

5. Dryer, A. M.; and Male, R. L.: Exciter-Regulator for the SNAP-8 Space Power System. IEEE Trans. on Aerospace, Supplement, vol. AS-3, no. 2, June 1965, pp. 560-567.

6. Edkin, Richard A.; Valgora, Martin E.; and Perz, Dennis A.: Performance Characteristics of a 15 kVA Homopolar Inductor Alternator for a 400 Hz Brayton-Cycle Space-Power System. NASA TN D-4698, 1968.

7. Bollenbacher, Gary; Edkin, Richard A.; and Perz, Dennis A.: Experimental Evaluation of a Voltage Regulator-Exciter for a 15-Kilovolt-Ampere Brayton Cycle Alternator. NASA TN D-4697, 1968.

8. Dryer, A. M.; Kirkpatrick, F. M.; Russell, E. F.; Wimsatt, J. M.; and Yeager, L. J.: Alternator and Voltage Regulator-Exciter Design and Development. Vol. I of Research and Development of High Performance Turboalternator and Associated Hardware. Pratt and Whitney Aircraft (Contract NAS3-6013), 1967.

9. Word, John L.; Fischer, Raymond L. E.; and Ingle, Bill D.: Static Parasitic Speed Controller for Brayton-Cycle Turboalternator. NASA TN D-4176, 1967.

10. Fischer, Raymond L. E.; and Droba, Darryl J.: Dynamic Characteristics of Parasitic Loading Speed Controller for 10 Kilowatt Brayton Cycle Turboalternator. NASA TM X-1456, 1968.

11. Greenwell, J. E.; Russell, E. F.; and Yeager, L. J.: Unbalanced Electromagnetic Forces Investigation. Vol. II of Research and Development of High Performance Turboalternator and Associated Hardware. Pratt and Whitney Aircraft Contract NAS3-6013), 1967.

12. Gilbert, Leonard J.: Reduction of Apparent-Power Requirement of Phase-Controlled Parasitically Loaded Turboalternator by Multiple Parasitic Loads. NASA TN D-4302, 1968.

TABLE I. - FINAL DESIGN

Stator:		Field:	
Turns per coil	4	Outside diameter, in. (cm)	8.68 (22.05)
Effective turns	26.55	Inside diameter, in. (cm)	6.48 (16.46)
Strands per turn	2	Turns	515
Circuits	2	Resistance at 160° C, ohms	4.97
Coil pitch	0.667	Field current at 15 kVA, A	6.29
Resistance at 160° C, per unit	0.0183	Gap, in. (cm)	0.40 (0.102)
Slots skewed	0	Materials:	
Slots	48	Rotor	AISI 4620
Dimensions, in. (cm):		Pole tips	AISI M-19 (0.014 in. (0.036 cm))
Length	4 (10.16)	Stator laminations	Silicon steel (0.007 in. (0.018 cm))
Slot pitch	0.346 (0.879)	Frame flanges	AISI 4140
Outside diameter	8.68 (22.05)	Frame shroud	72 percent Ni, 14 percent Cr, and 6 percent Fe
Inside diameter	5.28 (13.41)		
Yoke thickness	1.1 (2.79)	Windage baffles	AISI 321
Slot width	0.171 (0.434)	Frame	Ingot iron
Stack separation	2.2 (5.59)	Conductors	Tough pitch copper
Rotor:		Conductor insulation	Polymide enamel
Weight, lb (kg)	20 (9.07)	Impregnant	Epoxide compound
Dimensions, in. (cm):		Amortisseur bars	Zirconium copper
Length	3.9 (9.91)	Connection insulation	Polytetrafluoroethylene glass
Hub diameter	3.6 (9.14)	Slot liner	Polyimide film
Outside diameter	5.2 (13.21)	Separator	Silicone glass
Pole thickness	2.1 (5.33)	Topstick	Molded polyimide resin
Pole axial length	1.95 (4.95)	Electromagnetic weight, lb (kg)	82 (37.2)
Pole axial separation	2.2 (5.59)		
Pole arc	2.86 (7.26)		

TABLE II. - LOSS SUMMARY

[Load, 12 kW at 0.8 power factor; inlet coolant temperature, 93.4° C; argon pressure in cavity, 10.5 psia (7.245 N/cm^2 abs).]

	Design	Test
Loss[a], W		
Armature copper	276	277
Field copper	206	135
Core	200	320
Stray (include pole face)	190	270
Total electrical loss	892	1002
Windage loss	220	107
Total loss	1092	1109
Efficiency, percent	91.6	91.5

[a]Bearing loss not included.

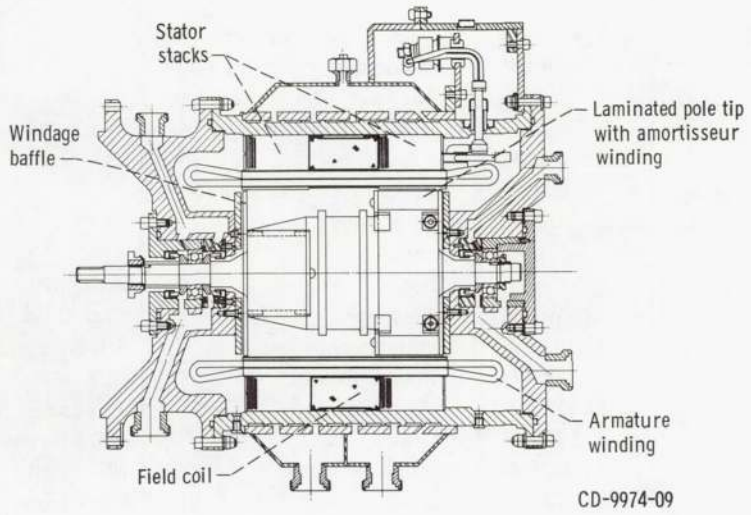

Figure 1. - Brayton-cycle test alternator.

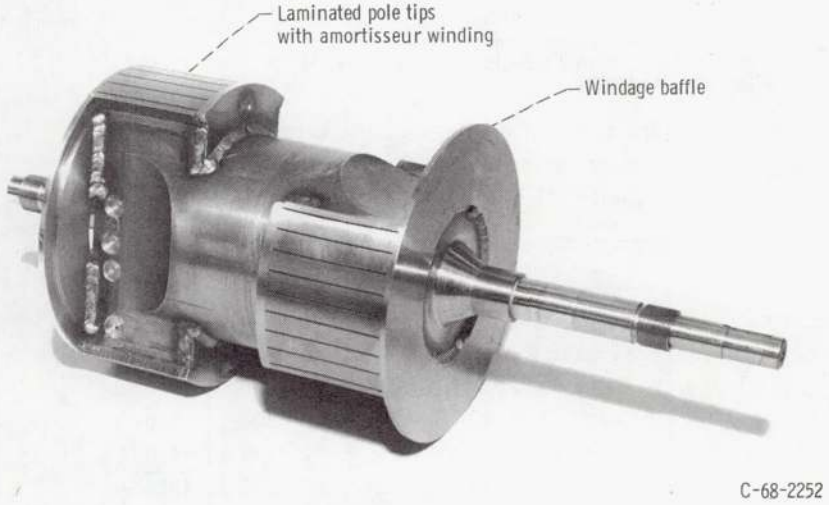

Figure 2. - Rotor of test alternator.

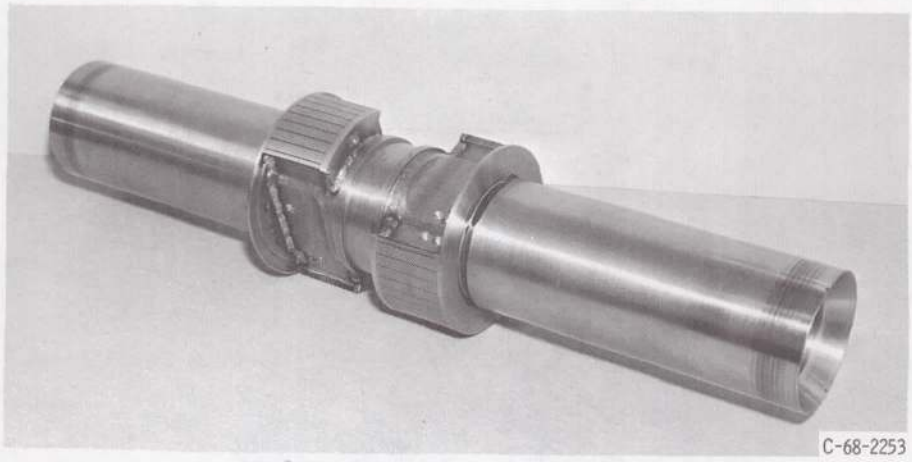

Figure 3. - Turboalternator rotor.

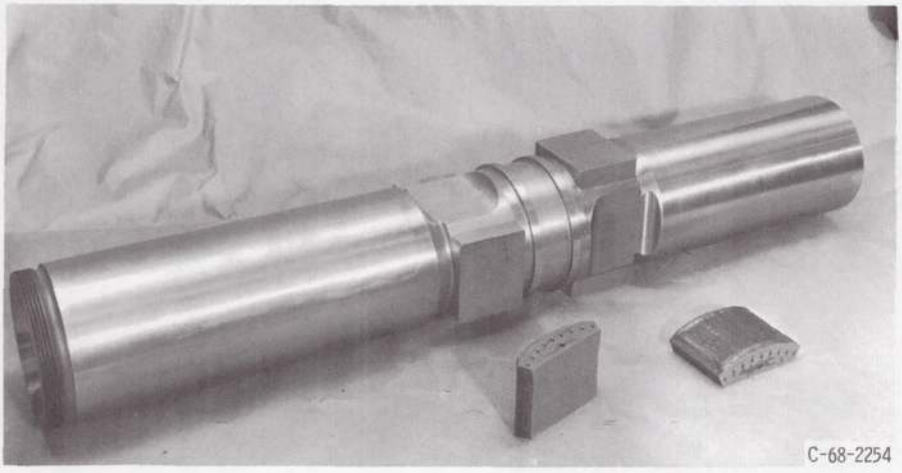

Figure 4. - Turboalternator rotor and laminated pole faces, before welding to rotor.

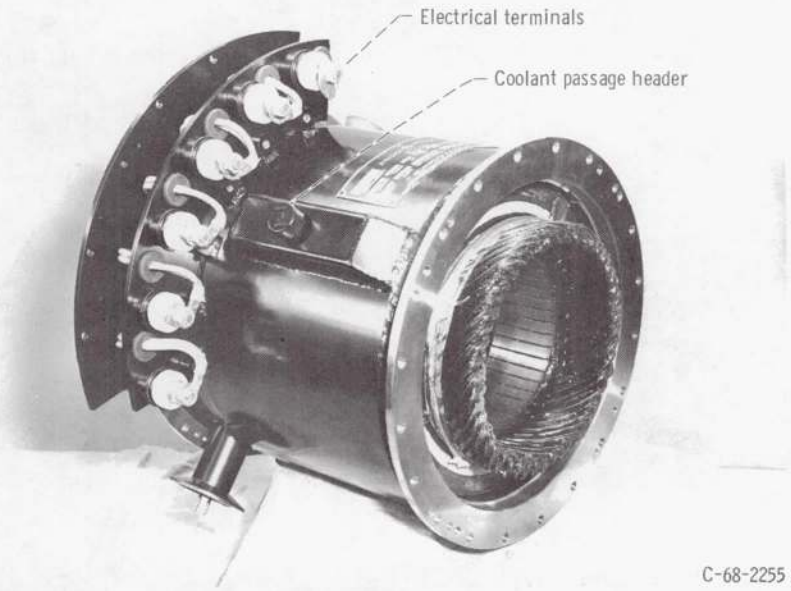

Figure 5. - Test alternator stator.

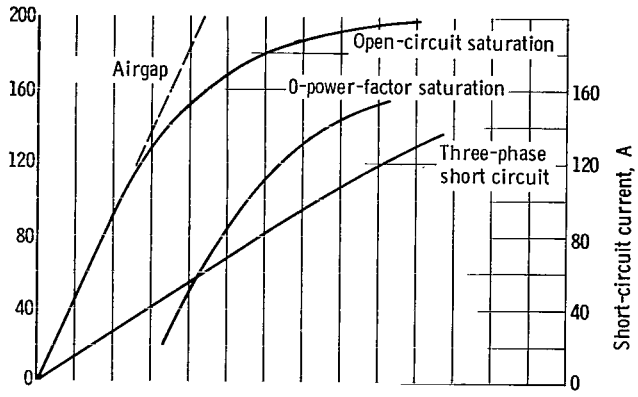

(a) Characteristic.

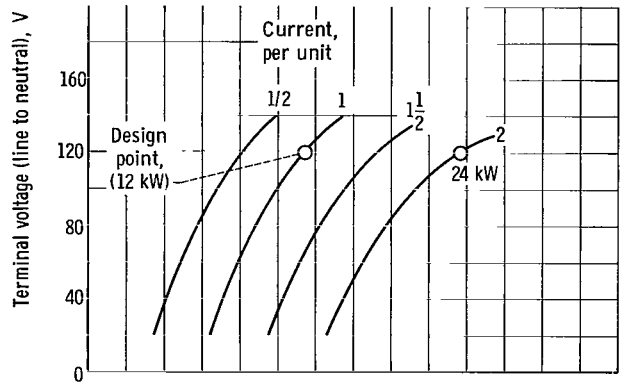

(b) Load saturation at 0.8 lagging power factor. (1 per unit current = 41.7 A).

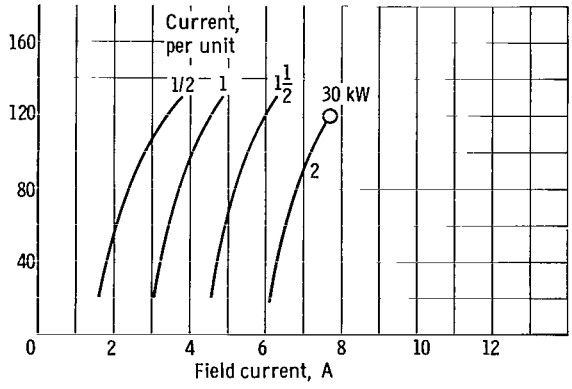

(c) Load saturation at 1 power factor. (1 per unit current = 41.7 A).

Figure 6. - Brayton-cycle alternator.

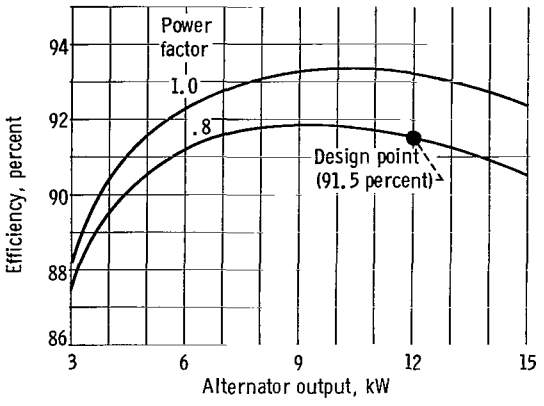

Figure 7. - Brayton-cycle alternator efficiency (bearing loss not included). Load, 15 kilovolt-amperes; inlet coolant temperature, 93.4° C; coolant flow rate, 1.66 gallons per minute (6.28×10^{-3} m^3/min).

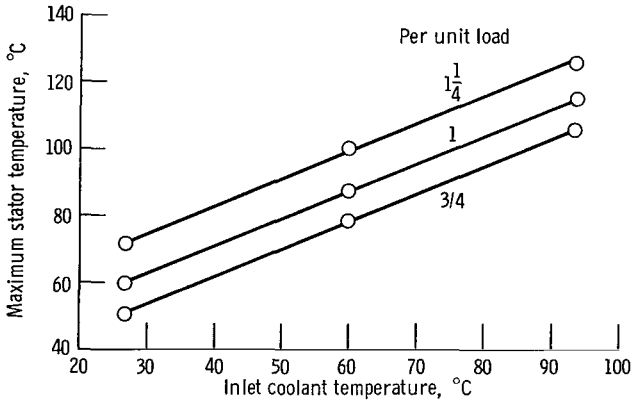

Figure 8. - Brayton-cycle alternator variation of stator temperature with inlet coolant temperature and 0.8-power-factor loads.

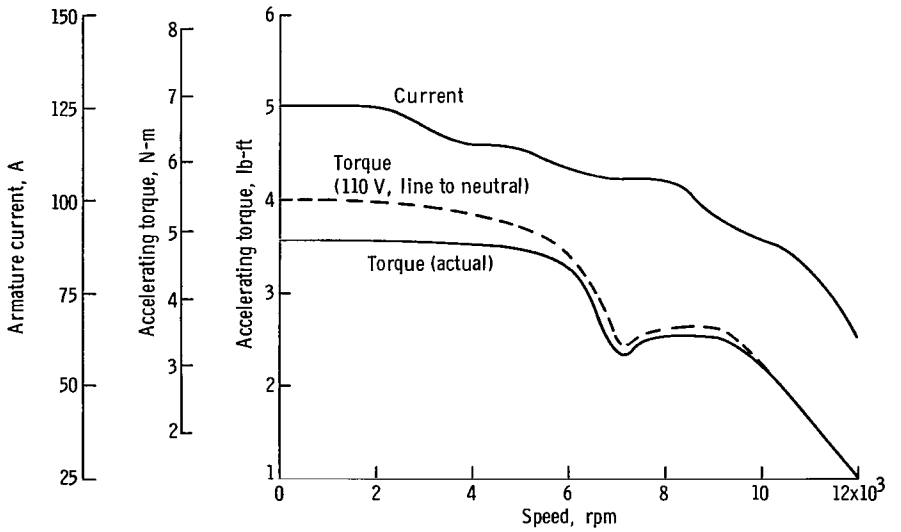

Figure 9. - No-load motor-starting characteristics for 400-hertz Brayton-cycle alternator.

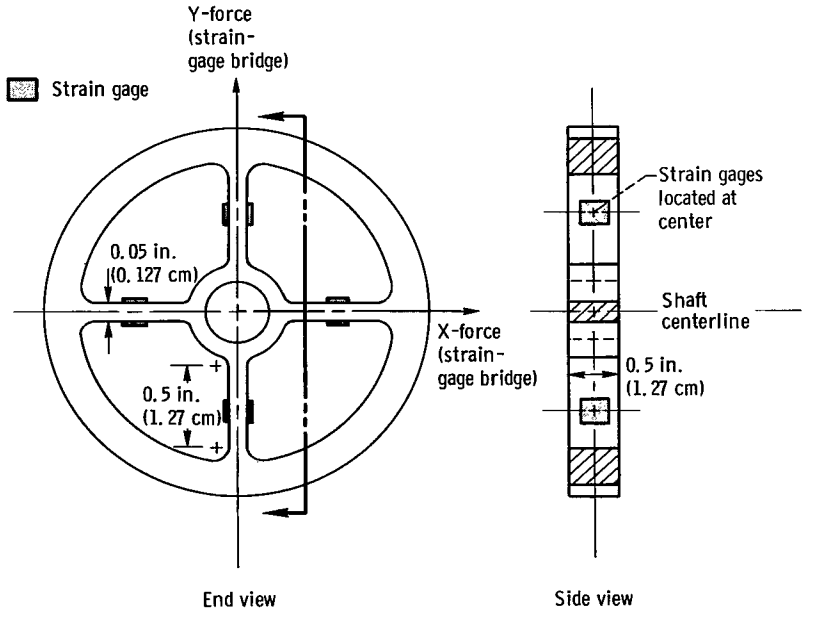

Figure 10. - Simplified end support. End shield material, 304 stainless steel.

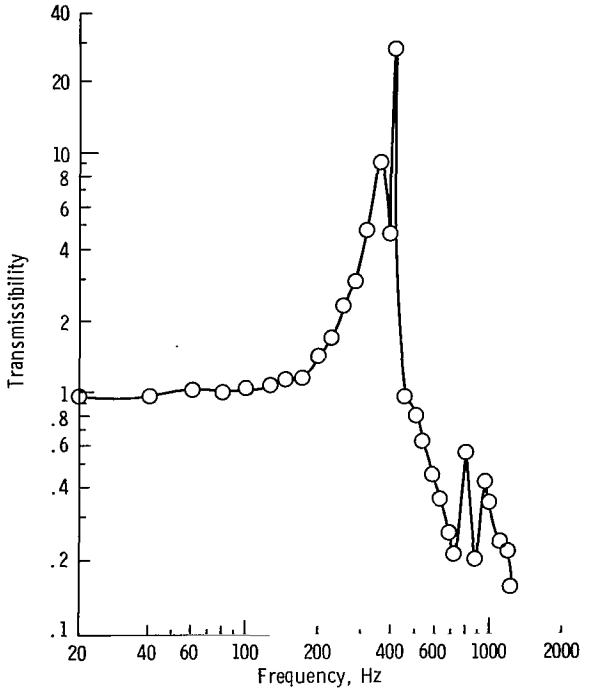

Figure 11. - Transmissibility from frame to rotor as function of frequency.

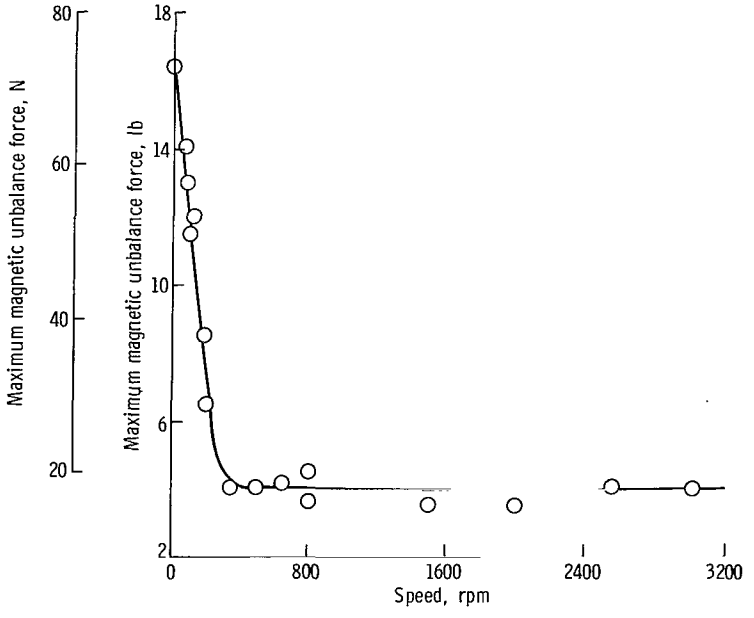

Figure 12. - Brayton-cycle alternator radial magnetic force at the drive end. No load; 2.7 field amperes; eccentricity, 0.004 inch (0.0102 cm).

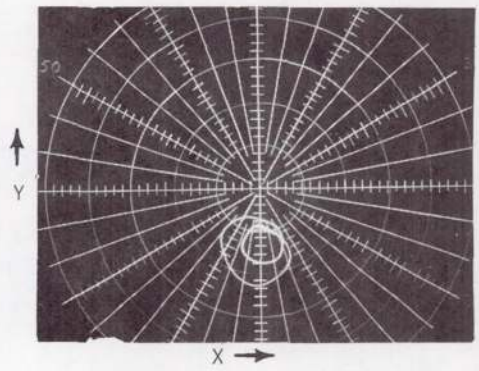

Polar plot of bearing forces

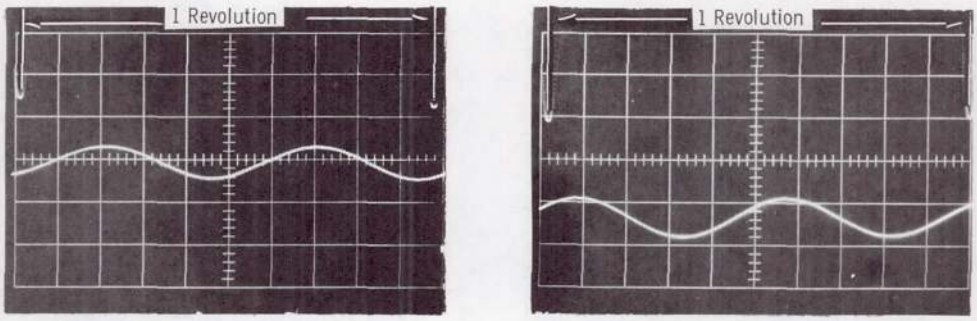

Constant force plus 100-hertz component.

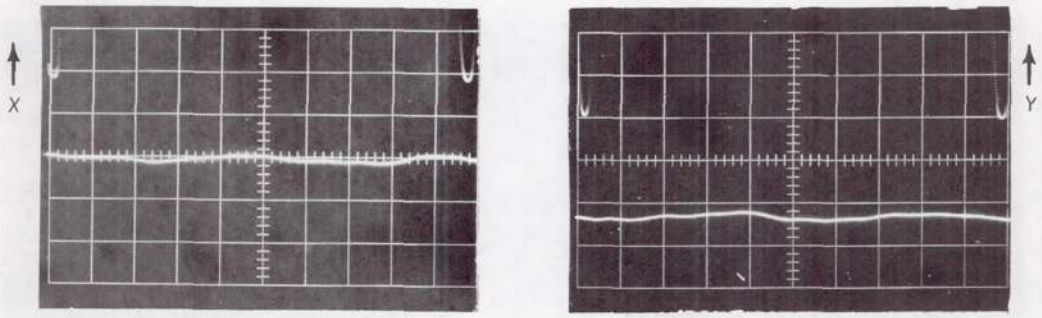

Constant force plus 200-hertz component.

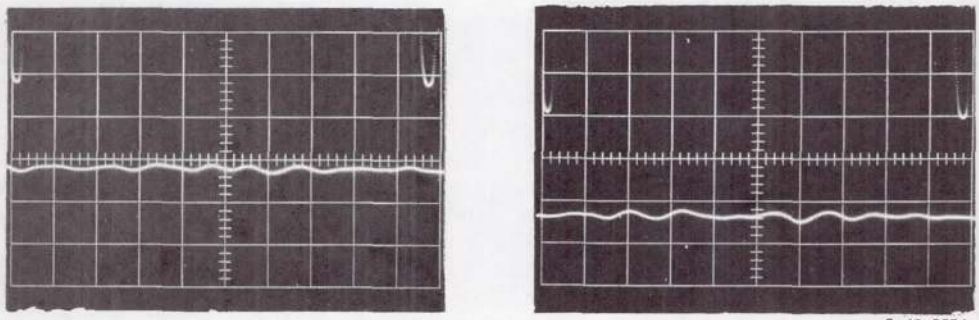

Constant force plus 300-hertz component.

(a) Balanced load; speed, 3000 rpm.

Figure 13. - Forces exerted on bearings of Brayton-cycle alternator. Eccentricity, 0.0063 inch (0.016 cm); equivalent load condition, 15 kilovolt-amperes, 0.8 power factor, three phase; location, drive-end bearing; force scale, 5 pounds (22.2N) per major division, radial or vertical; time scale, one revolution between timing marks.

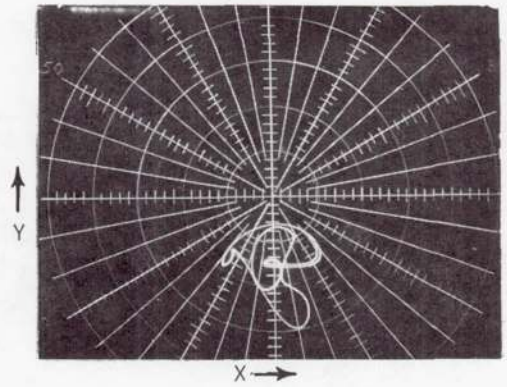

Polar plot of bearing forces

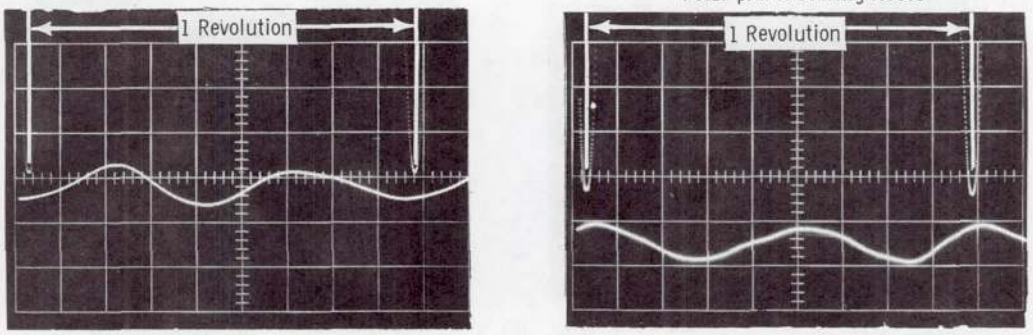

Constant force plus 115-hertz component.

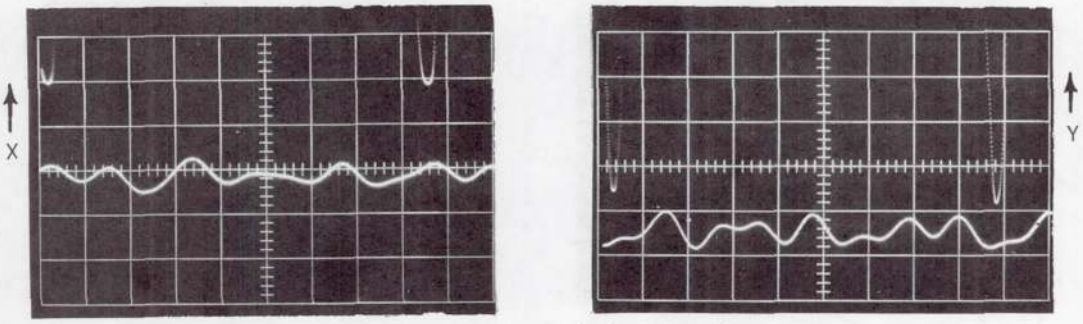

Constant force plus 230-hertz component.

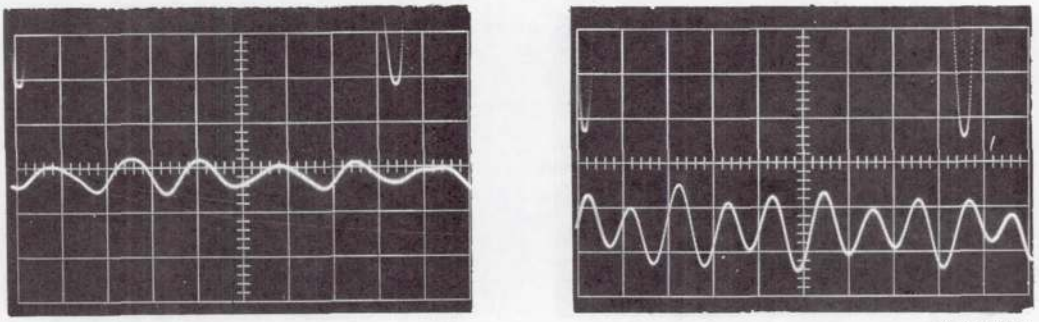

Constant force plus 345-hertz component.

(b) Single-phase fault; speed, 3450 rpm.

Figure 13. - Concluded.

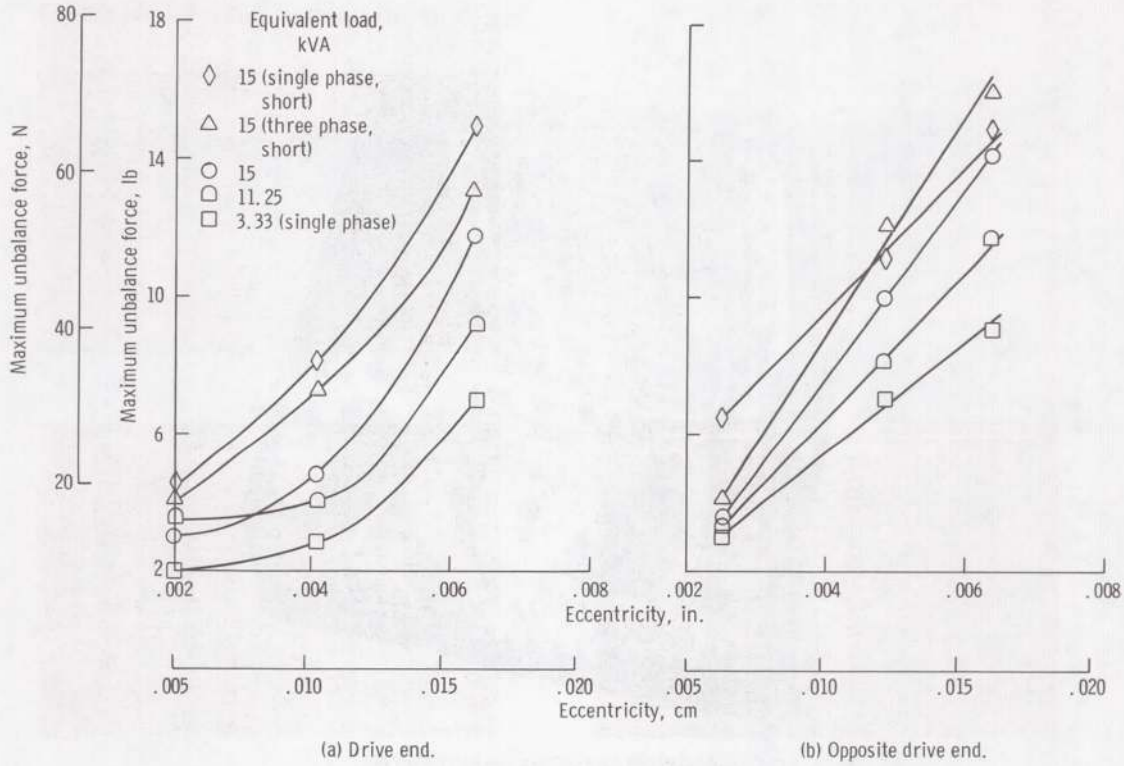

Figure 14. - Brayton-cycle alternator bearing reactions due to unbalanced flux.

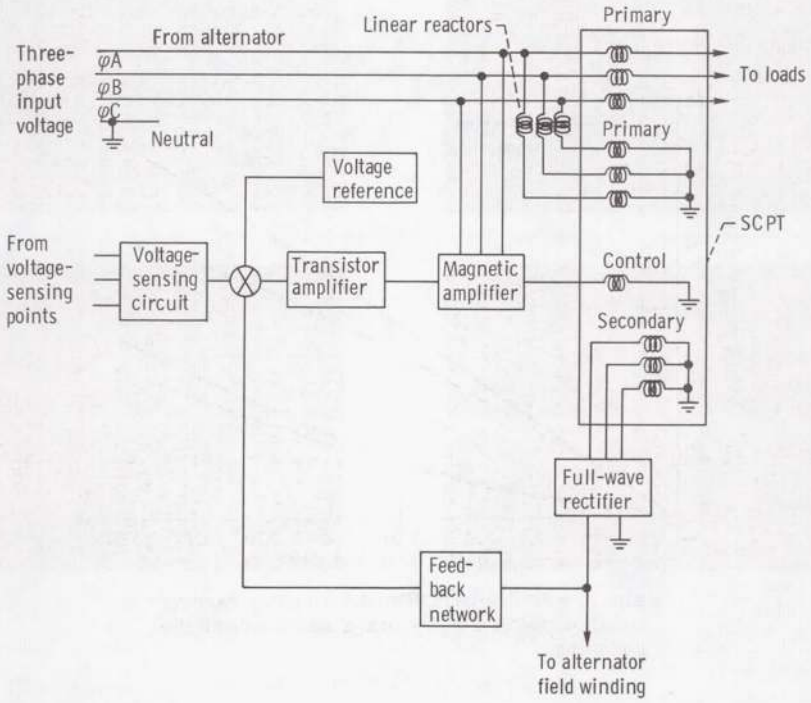

Figure 15. - Brayton-cycle voltage regulator - exciter block diagram.

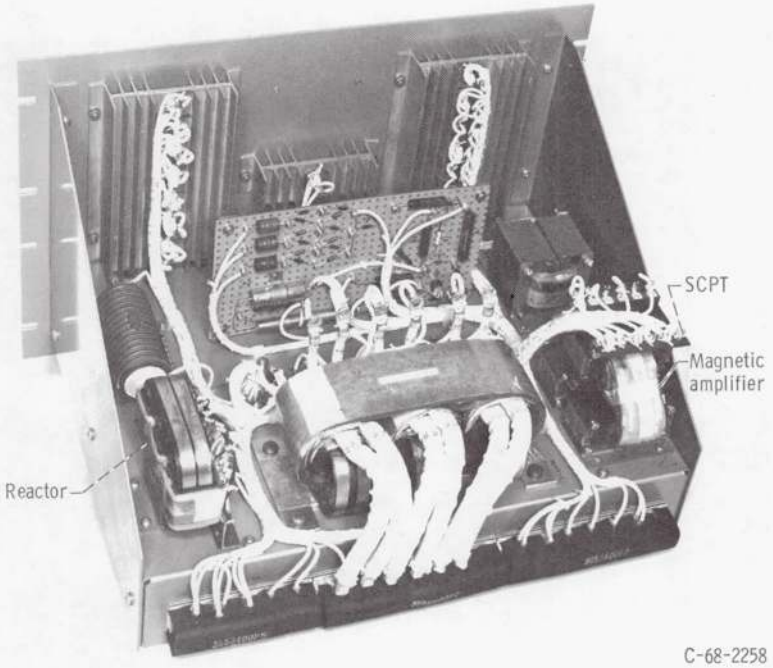

Figure 16. - Breadboard voltage regulator - exciter.

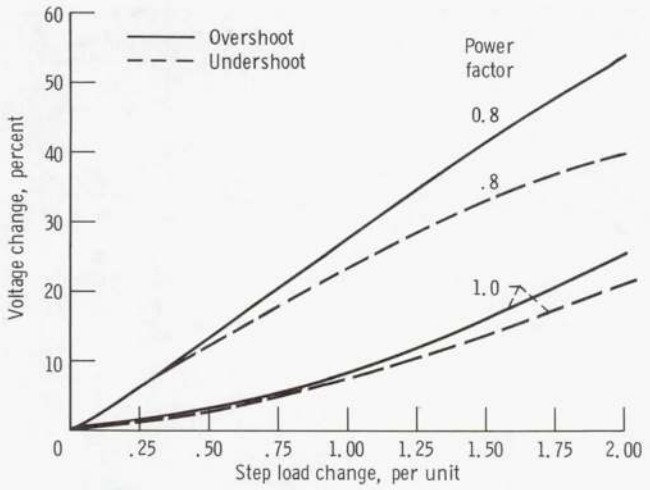

Figure 17. - Brayton-cycle alternator and voltage regulator - exciter percentage of voltage change against per unit step load change.

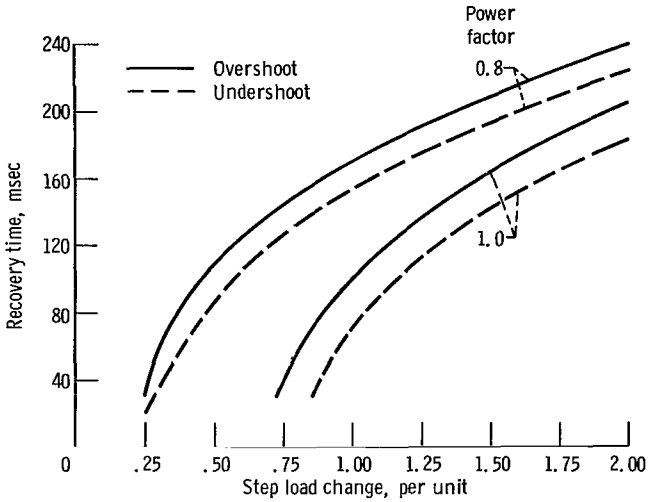

Figure 18. - Brayton-cycle alternator and voltage regulator transient recovery time against per unit step load change.

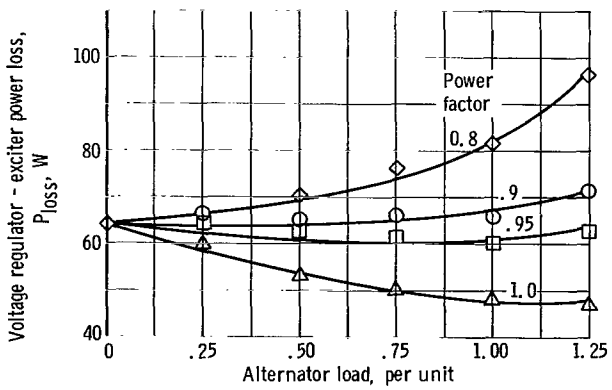

Figure 19. - Variation of voltage regulator - exciter losses with alternator load.

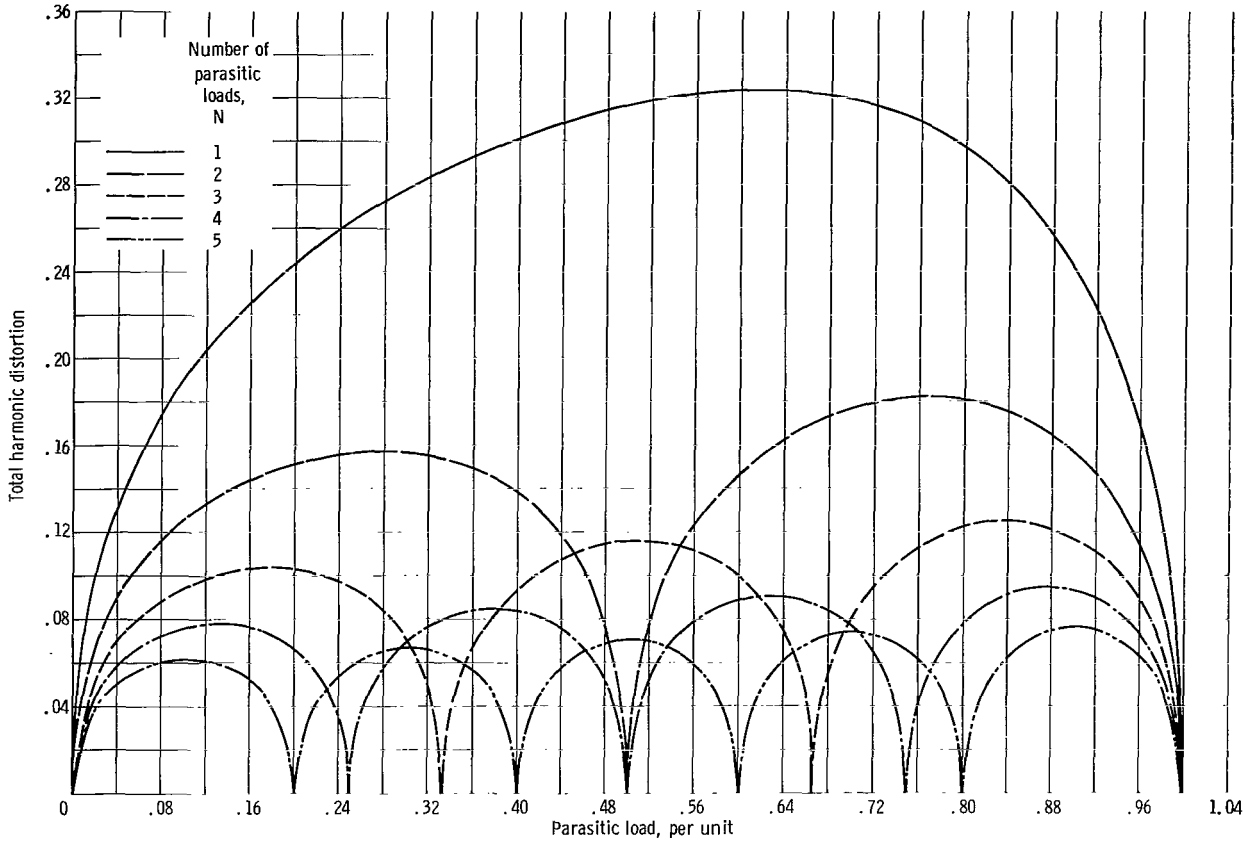

Figure 20. - Alternator current harmonic distortion for N parallel parasitic loads. Useful load power factor, 0.8 lagging.

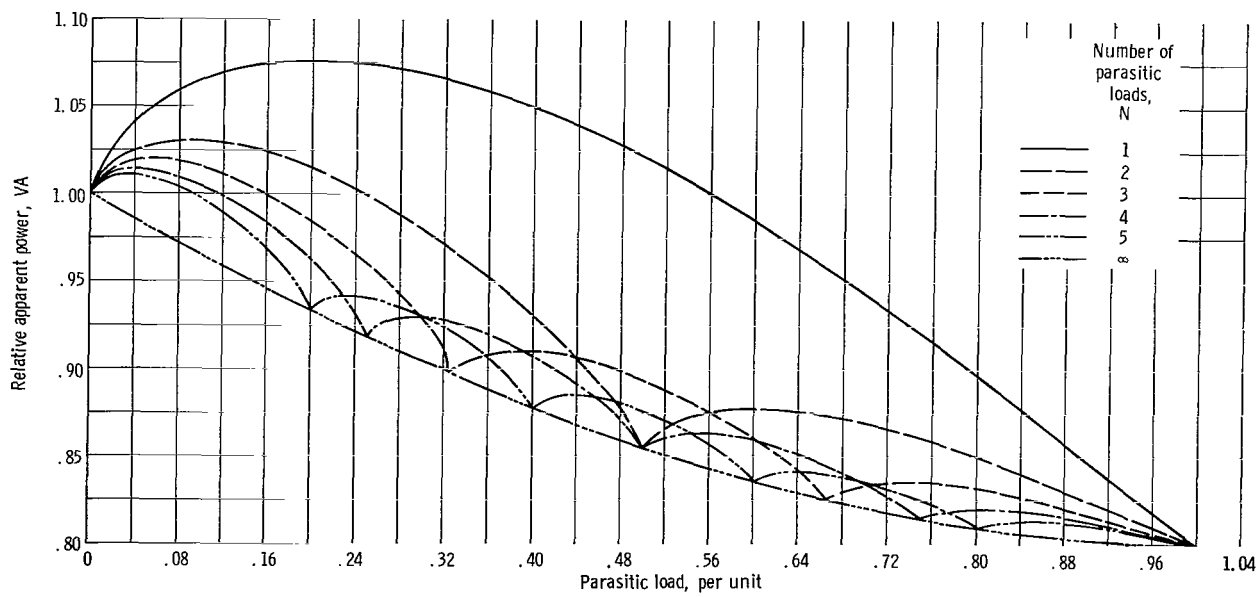

Figure 21. - Alternator apparent power required with N parallel parasitic loads relative to alternator rating without parasitic load. Useful load power factor, 0.8 lagging.

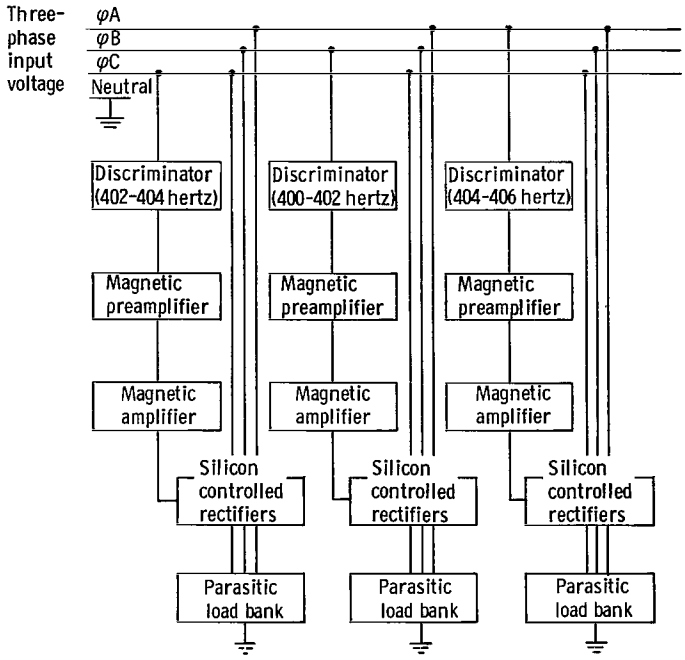

Figure 22. - Block diagram of Brayton-cycle speed controller.

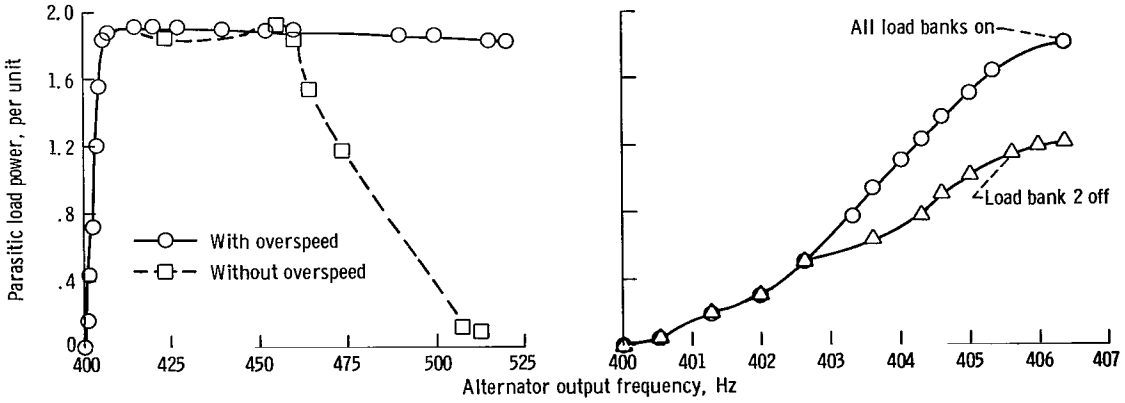

(a) Over full frequency range.

(b) Over expanded frequency range.

Figure 23. - Parasitic load power as function of alternator output frequency.

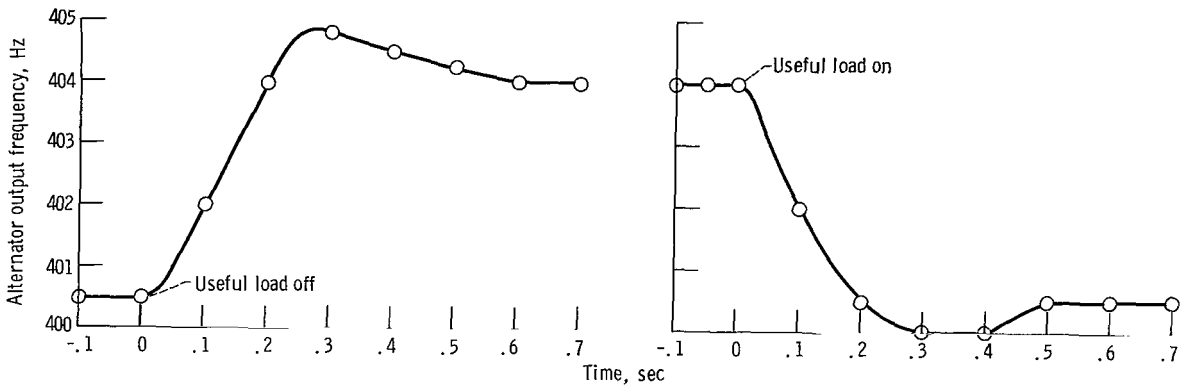

(a) Useful load stepped off, 1 per unit (13.8 kW).

(b) Useful load stepped on, 0.95 per unit (13.8 kW).

Figure 24. - Effect of step-increase in load on alternator frequency.

NASA-Langley, 1968 — 3 E-3999

NATIONAL AERONAUTICS AND SPACE ADMINISTRATION
WASHINGTON, D. C. 20546
OFFICIAL BUSINESS

FIRST CLASS MAIL

POSTAGE AND FEES PAID
NATIONAL AERONAUTICS AND
SPACE ADMINISTRATION

POSTMASTER: If Undeliverable (Section 158 Postal Manual) Do Not Return

"The aeronautical and space activities of the United States shall be conducted so as to contribute . . . to the expansion of human knowledge of phenomena in the atmosphere and space. The Administration shall provide for the widest practicable and appropriate dissemination of information concerning its activities and the results thereof."

—NATIONAL AERONAUTICS AND SPACE ACT OF 1958

NASA SCIENTIFIC AND TECHNICAL PUBLICATIONS

TECHNICAL REPORTS: Scientific and technical information considered important, complete, and a lasting contribution to existing knowledge.

TECHNICAL NOTES: Information less broad in scope but nevertheless of importance as a contribution to existing knowledge.

TECHNICAL MEMORANDUMS: Information receiving limited distribution because of preliminary data, security classification, or other reasons.

CONTRACTOR REPORTS: Scientific and technical information generated under a NASA contract or grant and considered an important contribution to existing knowledge.

TECHNICAL TRANSLATIONS: Information published in a foreign language considered to merit NASA distribution in English.

SPECIAL PUBLICATIONS: Information derived from or of value to NASA activities. Publications include conference proceedings, monographs, data compilations, handbooks, sourcebooks, and special bibliographies.

TECHNOLOGY UTILIZATION PUBLICATIONS: Information on technology used by NASA that may be of particular interest in commercial and other non-aerospace applications. Publications include Tech Briefs, Technology Utilization Reports and Notes, and Technology Surveys.

Details on the availability of these publications may be obtained from:

SCIENTIFIC AND TECHNICAL INFORMATION DIVISION

NATIONAL AERONAUTICS AND SPACE ADMINISTRATION

Washington, D.C. 20546